

# Computer Simulation of the Cryoprotectant Disaccharide $\alpha,\alpha$ -Trehalose in Aqueous Solution

Paul B. Conrad and Juan J. de Pablo\*

Department of Chemical Engineering, University of Wisconsin—Madison, 1415 Engineering Drive, Madison, Wisconsin 53706

Received: October 21, 1998

Protecting biological molecules during freezing and lyophilization is of commercial importance to the pharmaceutical, medical, and food industries. Much work has been done on the use of a wide variety of cryoprotectant compounds for these types of processes. Chief among these compounds are the saccharides. They have been found to protect proteins during freezing and drying stresses as well as prevent membrane damage during cooling of cells. Trehalose, a naturally occurring disaccharide of glucose, has been found to be a particularly effective cryoprotectant. Although there are several prevailing structural and thermodynamic arguments as to why molecules such as trehalose act as cryoprotectants, little fundamental work has been done to corroborate or refute these hypotheses. To address this issue, our work has focused on the structural and dynamic simulation of this promising cryoprotective system. In this work, we have implemented fully flexible, all-atom models for water and trehalose and used both Monte Carlo and molecular dynamics algorithms to calculate various macroscopic properties of trehalose solutions over a wide range of concentration. We have also studied the glass transition behavior at various concentrations and compared it to experimental data. We have observed the existence of intramolecular hydrogen bonding, which has been invoked to explain compressibility and molar volume data for concentrated solutions of trehalose. We have studied the diffusivity of water molecules in concentrated trehalose solutions and found a gradual transition from continuous motion through the matrix in more diluted systems to cavity-hopping motion in concentrated and near-glassy cases. Our diffusivity results have been analyzed in terms of the Williams–Landel–Ferry equation; good agreement is found with published glass transition data.

## 1. Introduction

Cryopreservation and freeze-drying processes have undergone considerable evolution in the past 50 years. In that time, a wide variety of substances have been used as cryoprotectants. These can be very broadly divided into two classes, those that permeate cells and those that do not. Of the permeating compounds, dimethylsulfoxide and glycerol are by far the most common. Nonpermeating compounds can come from many classes of molecules, including polymers, proteins, and saccharides.

Sugars have frequently been used for protecting both proteins and cells during freezing and drying.<sup>1,2</sup> A number of mechanisms have been suggested for their effectiveness. These include their ability to form glasses, to mimic the hydrogen bonding character of water, to increase the surface tension of the bulk solvent, to prevent thermotropic phase separations in lipid bilayers, and to prevent the fusion of membranes. One of the most promising saccharide cryoprotectants,  $\alpha,\alpha$ -trehalose, has only recently received more attention.

Trehalose is a nonreducing disaccharide of glucose; its structure is given in Figure 1. It occurs naturally in many organisms which suffer dehydration stresses (e.g., baker's yeast). Trehalose's success as a protectant has been attributed to its strong interaction with water and lipid membranes, its unique chemical stability, and its glass-forming behavior.<sup>3,4</sup> Figure 2 gives the current supplemented phase diagram for aqueous trehalose solutions.<sup>5–7</sup> The interactions between trehalose and

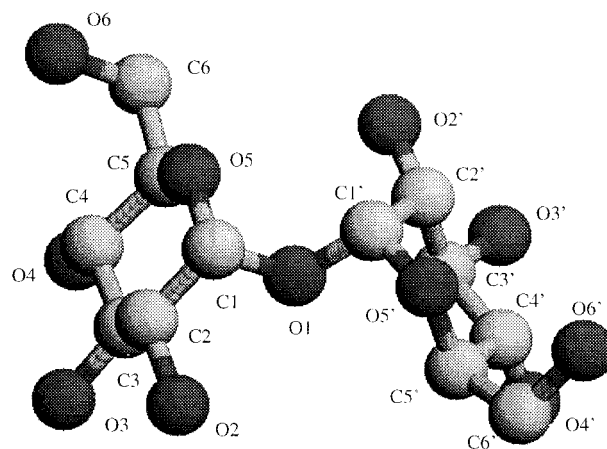


**Figure 1.**  $\alpha,\alpha$ -Trehalose. The hydrogen atoms have been left off for clarity. All carbon and oxygen atoms have been labeled.

water are dramatic, especially with regard to its glass transition. When just 10 wt % water is added to trehalose, the glass transition of the system plunges by nearly 100 °C. This effect is particularly important for freeze-drying applications and has bearing on the nature of trehalose's effectiveness as a protectant for biologicals.

In order to better define the nature of trehalose's cryoprotective ability, we have carried out extensive molecular studies of trehalose solutions via computer simulation. The first reported use of molecular simulation to study the behavior of trehalose in solution was by Donnamaria et al. in 1994.<sup>8</sup> These authors

\* To whom correspondence should be addressed (depablo@engr.wisc.edu).

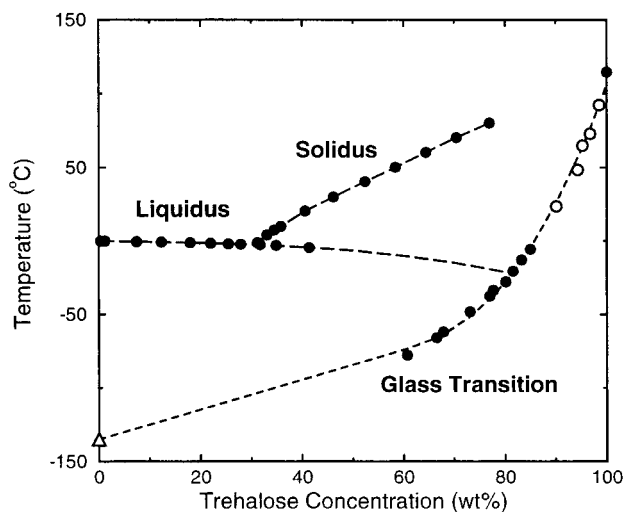


**Figure 2.** The phase diagram for trehalose in water. Note the dramatic reduction in glass transition temperature with the addition of small amounts of water to a pure trehalose system. The data are taken from refs 5 (●), 6 (○), 7 (△). The dashed lines are merely guides for the eye.

used a semirigid trehalose model with fixed bond lengths, harmonic bending potentials, and improper torsion potentials to fix the ring conformations. The only free rotation was about the glycosidic bond. This molecule was dissolved in SPC/E<sup>9</sup> water at 298 K. Their results indicated that trehalose was not well hydrated. This conclusion was surprising in light of a previous simulation of maltose which exhibited a high degree of hydrogen bonding with water.<sup>10</sup> Donnataria et al. also found that the formation of internal hydrogen bonds caused the molecule to twist in such a way that its hydroxyl groups roughly matched the placement of oxygen in a tetrahedrally coordinated water structure. Therefore, they concluded that the cryoprotective effect of trehalose was probably due to a “water replacement”<sup>11,12</sup> phenomenon at membrane and protein surfaces.

More recently, three other groups have challenged the first of Donnataria’s findings. Liu et al.<sup>13</sup> found that their trehalose model (based on the CHARMM potential<sup>14</sup>) had a high degree of hydration in TIP3P water. Sakurai et al.<sup>15</sup> used a flexible trehalose (developed from AMBER potential energy parameters<sup>16</sup>) with TIP3P water and found that trehalose was again strongly hydrated. In addition, Sakurai et al. found that, compared to maltose, trehalose has an extra site for hydrogen bonding which results in a slight decrease in the mobility of water bound to the sugar. A very recent work by Bonnanno et al.<sup>17</sup> has shown that their model for trehalose is also well hydrated by TIP3P with an average of 19 water molecules hydrogen bonded to it.

In the work presented here, special attention has been paid to the choice of model (force field) and the treatment of long-range interactions. The lack of hydration in the simulations of Donnataria et al. was likely due to potential energy parameters which were not well suited for the system. For our work, we have chosen to use the OPLS potential<sup>18</sup> which was developed for liquid systems and has recently been further optimized for all-atom simulations of carbohydrate solutions.<sup>19</sup> Our model is fully flexible, which is likely to be an important feature for study of dynamic processes near the glass transition. We have chosen to include long-range contributions to the energy and virial explicitly via an Ewald summation technique. The simulations of Liu et al. employed an arbitrary “switching function” to attenuate and turn off long-range interactions. Treatment of these interactions is not mentioned in the work by Donnataria et

al., Sakurai et al., or Bonnanno et al. Note that rigorous treatment of long-range interactions is known to have significant effects on the dynamic, structural, and thermodynamic properties of water and aqueous solutions.<sup>20</sup> More importantly, the scope of our work is considerably broader than that of previous studies which looked only at the behavior of trehalose in dilute solution at room temperature. We investigate a wide array of solution properties, dynamic aspects, and glass transitions in these systems. This required that we cover a broad range of temperatures and compositions. Only in this way can we begin to achieve a better understanding of the nature of trehalose and its properties.

## 2. Molecular Potentials and Simulation Details

In our work we use a fully-flexible SPC-type<sup>21</sup> water model developed by Toukan and Rahman.<sup>22</sup> Of the two models described in their work, the one with harmonic springs, was chosen in order to reduce computation time. The model for trehalose (see Figure 1) uses the OPLS force field, which was recently optimized for carbohydrates.<sup>19</sup> It is also a fully flexible, all-atom model which includes charges, Lennard–Jones interactions, and spring forces. The parameters for a bending interaction between an sp<sup>3</sup> carbon–ether oxygen–acetal carbon were used to approximate the bending at the glycosidic linkage. A detailed description of the implementation of the OPLS force field is given elsewhere.<sup>23</sup>

All of the models used in this work include Lennard–Jones 6–12, coulombic, and bonded interactions. The Lennard–Jones parameters were chosen from the references above; the cutoff distance in this work was at least 2  $\sigma$  (7 Å) for all atoms. The usual Lorentz–Bertholet combining rules were used to calculate cross-interaction parameters. A long-range correction was applied to the energy and virial to account for the truncation of the potential at the cutoff. The direct coulombic interactions (i.e., those within the Lennard–Jones cutoff radius) were calculated using an Ewald convergence parameter of 0.36 Å<sup>-1</sup>. Reciprocal space coulombic contributions were included by means of a “smooth particle mesh Ewald” (PME) method.<sup>24,25</sup> The PME method was used with eighth order splines and 16 mesh lines (spacing of 1.0–1.3 Å) in each dimension.

The simulations in this work were carried out using either an isothermal–isobaric Monte Carlo algorithm (NPTMC) or an isothermal molecular dynamics algorithm (NVTMD). Ensemble-specific simulation details are given below. The NPTMC algorithm was chosen because of its dependable performance even in simulations of dense systems such as aqueous solutions. The NPT ensemble, however, is known to converge rather slowly to equilibrium.<sup>26</sup> In order to speed the movement of the system through phase space, a hybrid Monte Carlo system was used<sup>27</sup> with a multiple time scales algorithm (r-RESPA).<sup>28</sup>

In hybrid Monte Carlo, instead of using random moves to displace molecules, the system is moved deterministically as in a conventional molecular dynamics simulation. The size of the time step can also be updated during the run to achieve the desired rate of acceptance for the displacement moves (70% in this work). This algorithm is attractive for highly complex molecules at relatively high densities because it allows for collective “moves” (in contrast to simple, random moves). Also, because it is a Monte Carlo formalism, it is an exact algorithm regardless of the time step chosen to displace the molecules. The reversible multiple time scales method (r-RESPA) was developed by Tuckerman et al.<sup>28</sup> to accelerate the performance of molecular dynamics simulations. This method involves a factorization of the normal velocity Verlet algorithm to allow

for more rapid updates of stiff or short-range interactions. In the case of the NPTMC work, the bonded and short-range interactions are updated five times for every update of the long-range interactions (i.e., the reciprocal space coulombic calculation). This technique was part of the hybrid Monte Carlo steps described above. As implemented for this work, a four-fold increase in the length of the overall time step (from 1 to 4 fs) was achieved by using hybrid Monte Carlo and r-RESPA as compared to traditional molecular dynamics.

The r-RESPA method was also used in the NVTMD calculations. In this case, however, a double RESPA method was employed to prevent deviation of the system pressure. The potential energy was separated into three parts: bonded interactions (includes bonds, bending, and torsion), short-range interactions (i.e., nonbonded interactions within the cutoff radius), and long-range interactions (i.e., reciprocal coulombic calculation). One step consisted of four updates of the bonded interactions, two updates of the short-range interactions and one update of the long-range interactions. The total time step used was 1 fs (i.e., the bonded and short-range interactions were updated every 0.25 and 0.5 fs, respectively). This value is small when compared to other reported implementations of the r-RESPA method but was necessary to obtain the correct pressure average and therefore the correct solvent structure for the flexible water model. This time step also eliminated the need for rigid bond constraints on the proton bonds. Included in this method was a chain of five Nosé–Hoover thermostats. Their inclusion into the r-RESPA methodology is described in ref 29. Following Nosé,<sup>30</sup> the frequency of the thermostat fluctuations was chosen to be  $0.002 \text{ fs}^{-1}$ . The box length for the NVTMD simulations was chosen from the density obtained in the NPTMC ensemble using a setpoint pressure of 0.1 MPa.

The system sizes depended on the concentration of the solution under investigation. For the most dilute case, 6 wt %, 300 water molecules were used with a single trehalose molecule. For the pure trehalose case, 10 or 20 molecules were used; the simulations with 20 molecules were used to investigate finite-size effects. Intermediate concentrations were between these two extremes. All of the NPTMC simulations were at least  $10^6$  steps, which included one hybrid displacement move (five MD-type steps) followed by one volume move. The lengths of the NVTMD simulations were at least  $2 \times 10^6$  steps (2 ns). Solutions closer to the glass transition required simulations as long as  $3.5 \times 10^7$  steps (35 ns) in order to reach the diffusive regime. The system densities ranged from 1.31 to  $1.44 \text{ g/cm}^3$  for the simulations of pure trehalose and from 1.13 to  $1.35 \text{ g/cm}^3$  for the simulations of 80 wt % solutions. The 98 wt % solution density was  $1.45 \text{ g/cm}^3$ . All volumes used in NVTMD simulations were determined from averages obtained during NPTMC simulations at the same temperature and a pressure of 0.1 MPa.

### 3. Results and Discussion

**3.1. Solution Properties.** We begin this section by comparing the results of our simulations to available experimental data. Density is a particularly important quantity in that it dictates how much “free volume” is available to each molecule in the system. The work of Cohen and Grest,<sup>31</sup> for example, relates this free volume for translational movement to diffusivity and viscosity (and, consequently, glass transition). As density increases, free volume decreases causing the diffusivity to decrease exponentially. This results in a higher viscosity and brings the system closer to its glass transition.

Our simulations of density were performed using the NPTMC method described above. The density was calculated for 0, 6,

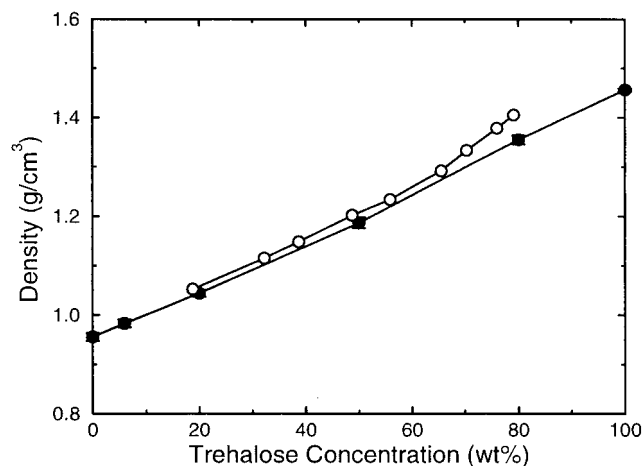


**Figure 3.** Trehalose solution densities from simulation at 85 °C. The solution densities of trehalose in water from simulation (●) as compared to experimental data from ref 32 (○). Note that the error bars on the simulated points are smaller than the symbols.

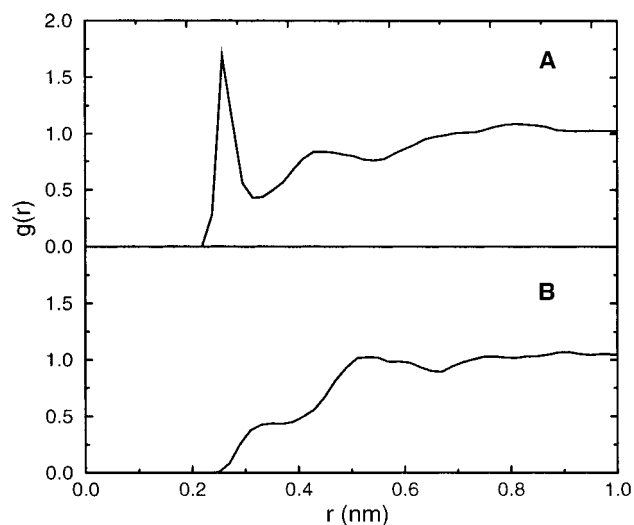


**Figure 4.** Hydration of trehalose oxygens. The radial distribution function for water oxygens around the hydroxyl oxygen attached to  $C_2$  (and  $C_2'$ ) (A) and around the ring oxygen  $O_5$  (and  $O_5'$ ) (B) for 6 wt % trehalose at 300 K. Panel A clearly shows hydrogen bond formation with a pronounced peak at 0.28 nm while the ring oxygen in panel B is not hydrated.

20, 50, 80, 90, and 100 wt % trehalose solutions at 85 °C. These results are compared to recent experimental findings<sup>32</sup> in Figure 3. The agreement between simulation and experiment is acceptable throughout the range of concentrations for which experimental data are available.

Another quantity of interest is the apparent molar volume of trehalose in solution. Based on the assumption of ideal mixing for the solvent, the apparent partial molar volume of the trehalose model ( $\bar{V}^\infty$ ) was found to approach  $208 \pm 1 \text{ cm}^3/\text{mol}$  at infinite dilution at 85 °C. This value is only slightly lower than that obtained from extrapolation of experimental data,<sup>33</sup> which place  $\bar{V}^\infty$  at  $216.7 \text{ cm}^3/\text{mol}$  for the same conditions. Again, the agreement between simulation and experiment is satisfactory.

**3.2. Trehalose–Water Interactions.** According to previous authors,<sup>8,15</sup> the hydroxyl groups of trehalose are well hydrated with well-defined nearest neighbor peaks in the radial distribution function between the trehalose hydroxyl oxygens and water oxygens ( $G_{O_t-O_w}$ ). Figure 4 presents  $G_{O_t-O_w}$  between water and a hydroxyl oxygen (Panel A) and a ring oxygen (Panel B) for a simulation of 6 wt % trehalose at 25 °C. The sharp peak at

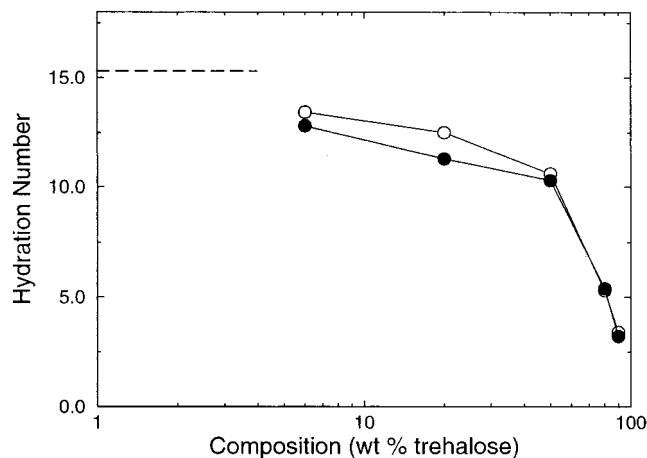


**Figure 5.** Composition dependence of trehalose hydration. Simulation results for average hydration number at 300 K (○) and 360 K (●). Simulation results compare well with published experimental results for infinitely dilute trehalose at 300 K (dotted line).<sup>34</sup>

2.8 Å in Panel A of Figure 4 indicates the presence of hydrogen bonding between the hydration waters and the hydroxyl group. The glycosidic oxygen has no such peak, and, therefore, is not hydrated.

To gain a better understanding of the nature of trehalose–water interactions, the level of hydration of trehalose was determined for various solution compositions. The presence of a hydrogen bond is noted when the two oxygen atoms approach within 3.4 Å and the angle formed between the donor oxygen–hydrogen–acceptor oxygen is 120° or greater.<sup>13</sup> As can be seen in Figure 5, the hydration number for trehalose, that is, the average number of waters hydrogen bonded per trehalose molecule over the course of the simulation, decreases monotonically from 12.8 at 6 wt % to 3.2 at 90 wt % at 85 °C and from 13.4 to 3.4 for the same range at 25 °C. This result compares favorably with ultrasound experiments that indicate the hydration number for trehalose is 15.3<sup>34</sup> for dilute solutions at 25 °C. It is interesting to note that using the criteria for hydrogen bonding given by Donnamaria et al., namely, 2.4 Å from proton to acceptor and an angle of 145° or greater, the hydration number for the most dilute sample (6 wt %) at 300 K decreases to 11.5.

**3.3. Molecular Conformation of Trehalose.** The presence of intramolecular hydrogen bonds was measured for a series of solutions at 85 °C. The criteria for internal hydrogen bonding was the same as that for bonding with water mentioned above. It was found that internal hydrogen bonds form at sugar concentrations of 50 wt % and above. The bonds occur between the O<sub>2</sub> and both the O<sub>5'</sub> and O<sub>5''</sub> oxygens (as well as the mirror image of these). An intramolecular probability distribution function between the O<sub>2</sub> and O<sub>6'</sub> was calculated for 20 wt % and 50 wt % solutions at 85 °C. Results are shown in Figure 6. Trehalose molecules spend a significant fraction of time in the internally hydrogen bonded configuration at high sugar concentrations. This is evident in Figure 7 which shows the distance between the O<sub>2</sub> and O<sub>6'</sub> oxygen atoms within a trehalose molecule in an 80 wt % solution at 85 °C. When the internal hydrogen bond forms, these two atoms approach to within 3.4 Å of each other. This clearly happens at several points during the 23 ns simulation in Figure 7. It is important to point out that the time scale for this behavior is extremely long. In fact, it is much longer than any of the other trehalose simulations reported in the literature, the longest of which was only 0.3 ns.<sup>17</sup>

The formation of intramolecular hydrogen bonds has recently been invoked to explain the increase in  $V^\infty$  with temperature,<sup>5</sup>

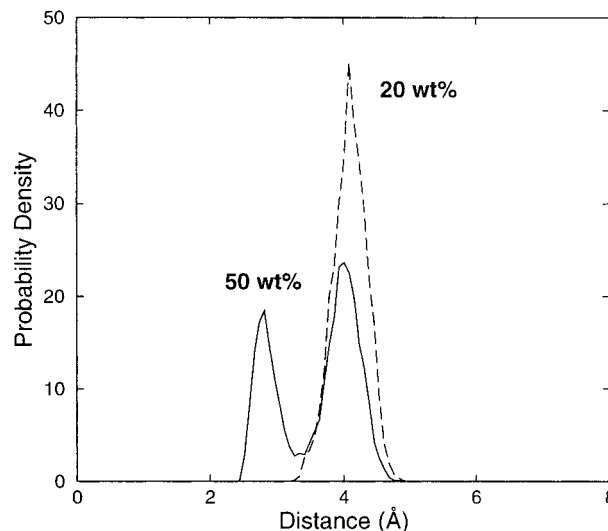


**Figure 6.** Intramolecular hydrogen bond formation for trehalose. The intramolecular probability distribution function for the O<sub>2</sub>–O<sub>6'</sub> interaction. Clearly, as trehalose concentration increases, the distribution exhibits a second peak. This peak's position at 2.8 Å indicates that it corresponds to a hydrogen bond.

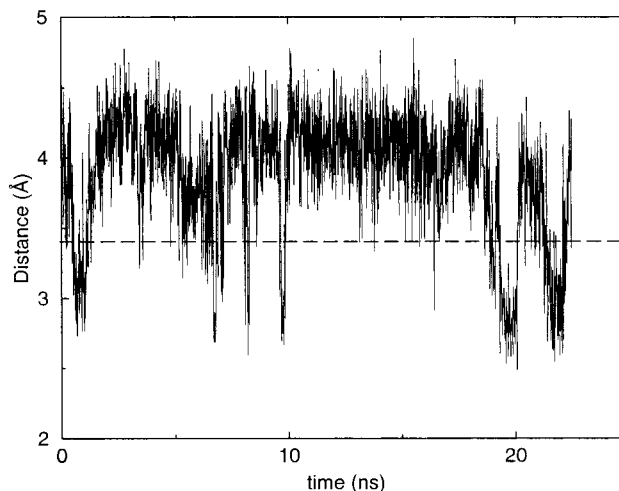


**Figure 7.** Interatomic distance between O<sub>2</sub>–O<sub>6'</sub>. The distance between the O<sub>2</sub> and O<sub>6'</sub> oxygens was monitored throughout a long NVTMD simulation of 80 wt % trehalose at 85 °C. Whenever the distance drops below 3.4 Å (dashed line), a hydrogen bond is formed if the angle criterion discussed in the main text has been met. This hydrogen bonding distance is achieved at several points in the simulation. The duration of these events is on the order of nanoseconds.

the change in sign of the isentropic compressibility with increasing sugar concentration at fixed temperature,<sup>32</sup> and the maximum in effective diffusivity observed at low sugar concentration.<sup>35</sup> A direct measurement of this “folding,” however, has not been made. This work confirms speculation that trehalose will satisfy in part its tendency to hydrogen bond by folding over on itself as water becomes scarce in the system.

**3.4. Glass Transitions of Trehalose Solutions.** Because the formation of trehalose glasses is of key importance for the use of trehalose as a cryo- and lyoprotectant, we estimated the presence and location of a glass transition for a pure system and for an 80 wt % solution. A series of trehalose simulations with descending temperatures was carried out. Each simulation was begun from the last configuration of the preceding (higher temperature) run. The glass transition was interpreted as the point at which the slope of the density versus temperature plot exhibits a discontinuity. As can be seen in Figure 8, this happens

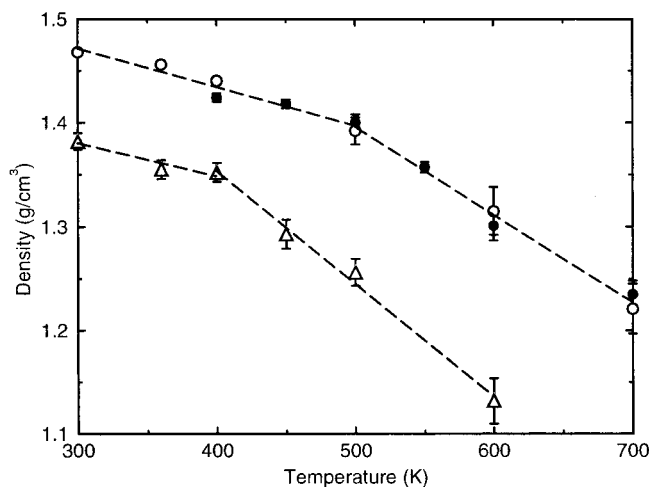


**Figure 8.** Glass transitions of trehalose solutions from simulation. The glass transition temperature is that point at which the slope of the density versus temperature curve experiences a discontinuity. Clearly this occurs near 500 K for pure amorphous trehalose (10 molecules  $\circ$  and 20 molecules  $\bullet$ ) and near 400 K for 80 wt % solutions ( $\Delta$ ).

near 500 K for a pure trehalose system (10 molecules) and near 400 K for solutions of 80 wt % trehalose (6 trehalose molecules with 29 waters). The same results were obtained from pure trehalose systems with 20 molecules, indicating that finite size effects are not seen in these results. The errors on the glass transition temperatures from this analysis are estimated to be  $\pm 40$  K. Note that the cooling rate from one point to the next was effectively infinite. The results from these simulations are therefore not expected to coincide with experimental data, as a fast cooling rate would result in a higher  $T_g$ . A highly accurate experimental measurement has recently been made by workers in our group which places the glass transition at 388 K for amorphous, anhydrous trehalose and at 246 K for 80 wt % solutions.<sup>5</sup> As expected, our ultrafast quench simulation results overpredict the transition in both cases, and the change in  $T_g$  with composition would appear to be slightly less pronounced for the model. In the following section, however, we revisit the glass transition behavior by analyzing several dynamic properties of the system.

**3.5. Diffusivity.** Diffusivity was measured for dilute trehalose (6 wt %), 80 wt %, and pure trehalose at a variety of temperatures from NVTMD simulation. The diffusivity calculation is based on the Einstein relation:

$$D = \lim_{t \rightarrow \infty} \frac{1}{6tn} \sum_n [x(0) - x(t)]^2 \quad (1)$$

where  $D$  is the diffusivity,  $t$  is time,  $n$  is the number of molecules, and  $x$  is the position of the center of mass as a function of time. A representative log-log plot of mean-squared displacement of trehalose versus time for 6 wt % trehalose at 25 °C is shown in Figure 9. From this data, the diffusivity for trehalose was calculated to be  $3.2 \times 10^{-6}$  cm<sup>2</sup>/sec, which compares well with the value of  $2.5 \times 10^{-6}$  cm<sup>2</sup>/sec which was interpolated from recently published experimental work.<sup>35</sup>

From a practical point of view, calculations for pure trehalose and for an 80 wt % solution are more relevant than those for dilute solutions, as they are concerned with the rate at which water diffuses in a freeze-dried trehalose sample. These results are presented in Figure 10. Not surprisingly, the diffusivity of trehalose in the pure system is roughly two orders of magnitude below that in a hydrated system (80 wt % trehalose). Also, in

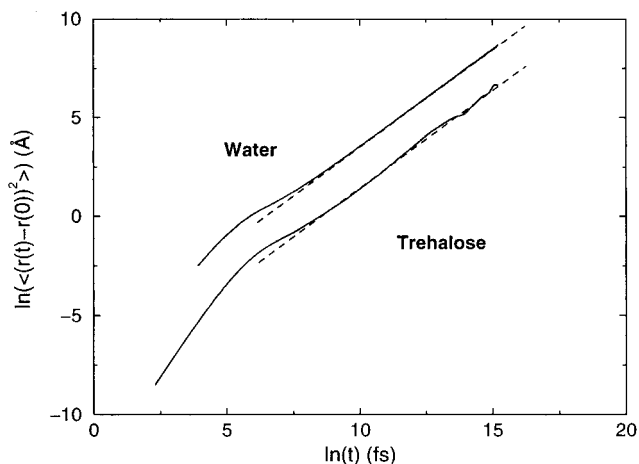


**Figure 9.** Log-log plot of mean-squared displacement versus time for trehalose and water (as labeled) in a 6 wt % trehalose solution at 25 °C. Once the molecules reach the diffusive regime, the slope of the curve is unity; its intercept is  $\ln(6D)$ . The dotted lines have unit slope.

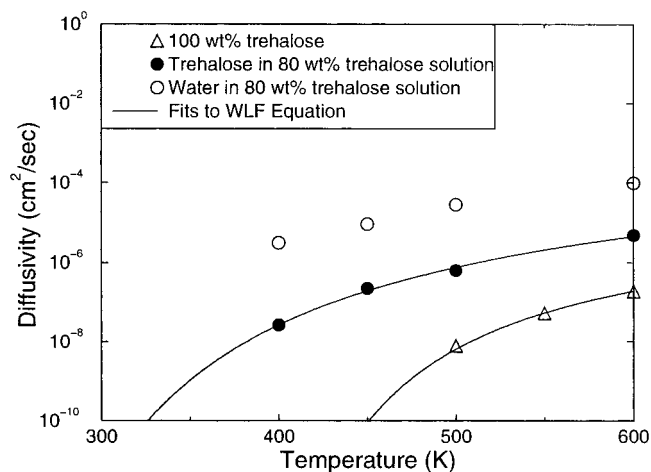


**Figure 10.** The diffusivity calculated for trehalose and water in solution. The behavior with temperature of trehalose diffusivity in a pure system is compared to trehalose and water in an 80 wt % trehalose solution. The trehalose data has also been fit with the WLF equation by using the Stokes-Einstein approximation to calculate viscosity.

the 80 wt % samples, the diffusivity of water remains about 30-fold higher than that of trehalose over a 250 degree range in temperature. As the trehalose becomes more hydrated, the effect of water becomes more pronounced, resulting in a 100-fold increase in trehalose diffusivity when 20 wt % water is reached (see circles in Figure 10).

Our calculations indicate that, for the concentrated systems studied in this work which are nearest (but still above) their glass transition temperatures, an unusually long equilibration time is required for the water to reach the diffusive regime. This is apparently due to restriction of the motion of water in these systems. The time scale of motion for the trehalose matrix has decreased to such an extent that the water molecules rattle around a specific site at short times, and they must wait for the trehalose molecules to move before they can jump to another site. An example of the slowed motion of the trehalose molecules is given in Figure 11 for a simulation of 98 wt % trehalose. In this case, the sugar molecules never reached the diffusive regime even after 30 ns of simulation time. In Figure 12 the path taken for a single water molecule in 98 wt % trehalose at 450 K is shown. For comparison, paths for water molecules in 80 wt % solutions at 450 and 600 K are also shown. It is clear that the water molecules are being trapped in

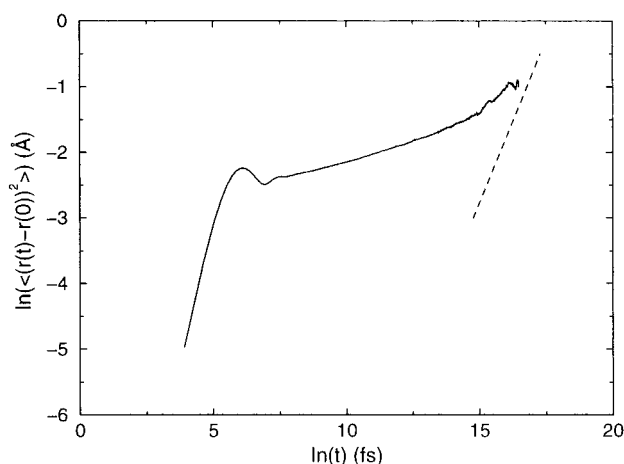


**Figure 11.** Log–log plot of mean-squared displacement versus time for trehalose in a 98 wt % trehalose solution at 177 °C. Even after 30 ns of simulation time, the trehalose has not reached the diffusive regime (i.e., the slope has not reached unity). The dotted line has unit slope.

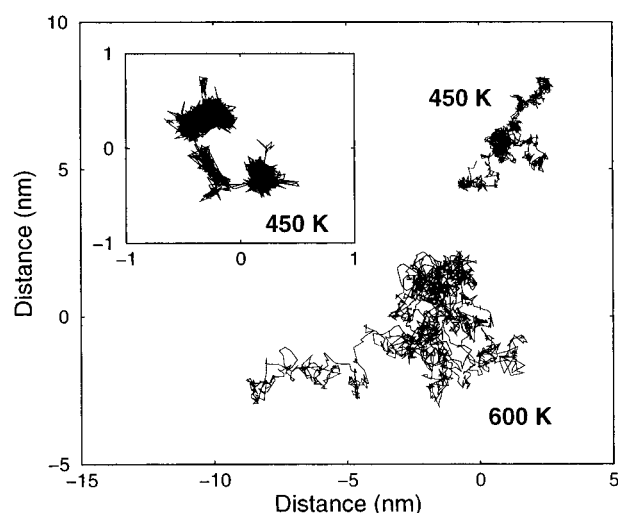


**Figure 12.** Comparison of water mobility in trehalose solutions. The movement of representative water molecules in 80 wt % trehalose solutions at 450 K and 600 K projected onto the  $X$ – $Y$  plane (main panel). This is compared to the movement of water in a 98 wt % trehalose solution at 450 K (inset panel). Note the change in scale for the inset and the fact that the 98 wt % simulation at 450 K was five times as long.

“pockets” from which they seldom escape. The path shown for the 98 wt % system can be seen to “hop” between three distinct cavities within the trehalose matrix. For water in 80 wt % trehalose at the same temperature, some incipient hopping which slows the motion of the water is apparent in Figure 12; at 600 K this behavior has entirely disappeared. This effect is similar to that originally described by Sok et al.<sup>36</sup> and Suter et al.<sup>37</sup> in which simulations of gas molecules dissolved in polymer membranes showed a distinct hopping mechanism as they moved from one pocket in the polymer matrix to another. This hindered motion gives rise to an “anomalous” diffusive regime, as shown in Figure 13 for an 80 wt % solution at 85 °C (360 K). The molecules in our system are being hindered by the formation of transient “cages” around them which results in a flat plateau region at intermediate times in the mean-squared displacement versus time plot.<sup>38</sup> This type of behavior has also been reported for simulations of gases in polymer glasses.<sup>37,39</sup>

Another interesting feature apparent in Figures 11 and 13 is the so-called “boson” peak in the mean-squared displacement at about  $\ln(t) = 6.25$  (0.5 ps). This peak was observed only in

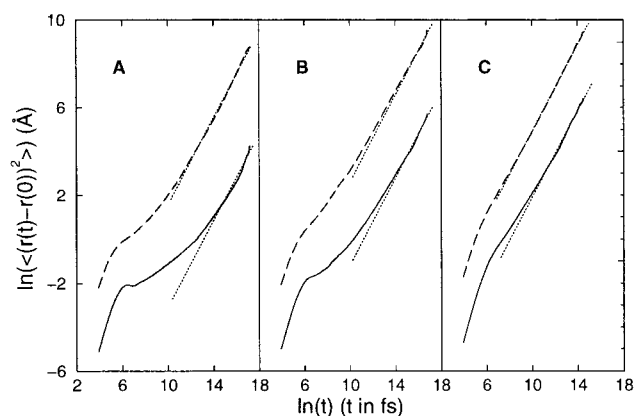


**Figure 13.** Log–log plot of mean-squared displacement versus time for trehalose (solid line) and water (long dashed line) in an 80 wt % trehalose solution at 127 °C (400 K) (panel A), 177 °C (450 K) (panel B), and 327 °C (600 K) (panel C). Once the molecules reach the diffusive regime, the slope of the curve is unity (dotted lines); its intercept is  $\ln(6D)$ . An interesting feature in panel A is the boson peak in the displacement of trehalose at  $\ln(t) = 6.25$  or the 500 ps time scale. This phenomenon is described more in the text.

the samples closest to their glass transition, namely, 80 wt % trehalose at 360 and 400 K as well as 98 wt % trehalose at 450 K. The appearance of a boson peak is considered indicative of a strong glass-forming system.<sup>40,41</sup> By way of comparison, our boson peak occurs at time scales slightly longer than those reported for silica<sup>42</sup> (0.6 ps versus 0.2 ps). It should be noted that the presence and size of the peak is strongly system size dependent.<sup>38</sup>

It is useful to examine our results in the framework of the Williams–Landel–Ferry (WLF)<sup>43</sup> equation, which is often used to describe the behavior of solutions of large molecules and polymers near their glass transition temperature. The equation has the form:

$$\log \eta/\eta_g = \frac{-C_1(T - T_g)}{C_2 + (T - T_g)} \quad (2)$$

where  $\eta$  and  $\eta_g$  are the viscosities at temperatures  $T$  and  $T_g$  and  $C_1$  and  $C_2$  are “universal” constants with values of 17.44 and 51.6, respectively. To use the form of this equation to fit our results, the viscosity of trehalose was first estimated via the Stokes–Einstein relation:

$$\eta = \frac{k_b T}{6\pi r D_t} \quad (3)$$

where  $k_b$  is Boltzmann’s constant,  $T$  is temperature, and  $r$  is the hydrodynamic radius of the diffusing particle. Based on the average radius of gyration of the simulated molecules, the hydrodynamic radius was estimated at 3.4 Å. For 80 wt % solutions,  $r$  was estimated as the radius of gyration of trehalose plus the first hydration shell. This value was 4.2 Å. The relation for  $\eta_g$  developed by Soesanto and Williams from concentrated solutions of fructose and glucose was also used:<sup>44</sup>

$$\log \eta_g = 1.918x_t + 11.021 \quad (4)$$

where  $\eta_g$  is in Pa-s and  $x_t$  is the mole fraction of trehalose. With this information, a nonlinear WLF-type regression was applied to the results in Figure 10. In this analysis, the experimental glass transition values<sup>5</sup> were used (388 K for pure trehalose, 247 K for 80 wt %) and the constants  $C_1$  and  $C_2$  were treated as fitting parameters. For the pure trehalose system,  $C_1$

and  $C_2$  were 15.41 and 31.41. For 80 wt % trehalose, they were 16.10 and 53.91. As can be seen from Figure 10, the WLF equation can describe our data reasonably well. We also analyzed our results using  $C_1$ ,  $C_2$  as well as  $T_g$  as fitting parameters. In this case the  $C_1$  values change only slightly, the  $C_2$  values increased somewhat, and the resulting  $T_g$  values are 371 K for pure trehalose and 235 K for the 80 wt % glass. These  $T_g$ 's are much closer to the experimental values than the density-temperature results given above, and the only inputs were the Soesanto-Williams viscosities (eq 4) along with our results for diffusivity, radius of gyration, and temperatures above  $T_g$ .

#### 4. Conclusions

We have shown in the sections above that our molecular model for trehalose can accurately reproduce many experimentally observed physical properties of trehalose solutions. This has allowed us to move forward and begin looking at the detailed molecular interactions that occur between trehalose and water as well as within the trehalose molecule itself. We have provided hydration numbers for trehalose which are, based on a detailed, microscopic model; prior to this work, such numbers could only be inferred from relatively coarse models applied to experimental data. Perhaps most interesting of these results is the confirmation of the presence of an internal hydrogen bond in trehalose at high concentration. This behavior had been invoked to explain compressibility and molar volume data for concentrated solutions of trehalose; our molecular simulations lend credence to that hypothesis. We have also investigated the behavior of the model system near the glass transition which we have evaluated using two independent means, namely, density profiles and fitting diffusivities with the WLF equation. By using a WLF-type analysis of diffusivity, we have reproduced the experimental glass transition temperature for two concentrated solutions. Diffusivity data for water in concentrated trehalose samples is of utmost importance for design of pharmaceutical formulations. Such data, however, are not available. Our predictions for diffusivity therefore serve to fill that gap in the literature. It is worth noting that we have observed the presence of a boson peak in the diffusive behavior of trehalose in the simulations which were closest to their  $T_g$ . Interestingly, we have also observed an apparent trapping of water molecules in the trehalose matrix as the system approaches  $T_g$ , which resembles that found in glassy polymers. On the basis of these preliminary findings, we are very hopeful that future work will shed more light on the nature and implications of the cryoprotective ability of trehalose and its behavior in multi-component systems for which there is an even greater lack of data.

**Acknowledgment.** For financial support of the work, the authors are grateful to the Biotechnology Training Program sponsored by the National Institutes of Health, to the National Science Foundation for a PECASE award, and to the Dreyfus Foundation for a Teacher-Scholar Award. J.J.dP. is also grateful to the Mexican Petroleum Institute for their hospitality while this work was in progress.

#### References and Notes

(1) Carpenter, J. F.; Prestrelski, S. J.; Arakawa, T. *Arch. Biochem. Biophys.* **1993**, *393*(2), 456-464.

- (2) Crowe, J. H.; Crowe, L. M.; Carpenter, J. F.; Rudolph, A. S.; Wistrom, C. A.; Spargo, B. J.; Anchodoguy, T. J. *Biochim. Biophys. Acta* **1988**, *947*, 367-384.
- (3) Roser, B. *Trends Food Sci. Tech.* **1991**, July, 166-169.
- (4) Green, J. L.; Angell, C. A. *J. Phys. Chem.* **1989**, *93*, 2880-2882.
- (5) Miller, D. P.; de Pablo, J. J.; Corti, H. *Pharm. Res.* **1997**, *14*(5), 578-590.
- (6) Saleki-Gerhardt, A. Ph.D. Thesis, University of Wisconsin, 1993.
- (7) Franks, F. In *Water and Aqueous Solutions at Subzero Temperatures*; Franks, F., Ed., Vol. 7 of *Water: A Comprehensive Treatise*; Plenum Press: New York, 1982; p 484.
- (8) Donnamaria, M. C.; Howard, E. I.; Grigera, J. R. *J. Chem. Soc., Faraday Trans.* **1994**, *90*(18), 2731-2735.
- (9) Berendsen, H. J. C.; Grigera, J. R.; Straatsma, T. P. *J. Phys. Chem.* **1987**, *91*, 6269-6271.
- (10) Brady, J. W.; Schmidt, R. K. *J. Phys. Chem.* **1993**, *97*, 958-966.
- (11) Crowe, J. H.; Crowe, L. M.; Carpenter, J. F. *Biopharm* **1993**, *6*(3), 28-32.
- (12) Crowe, J. H.; Crowe, L. M.; Carpenter, J. F. *Biopharm* **1993**, *6*(4), 40-43.
- (13) Liu, Q.; Schmidt, R. K.; Teo, B.; Karplus, P. A.; Brady, J. W. *J. Am. Chem. Soc.* **1997**, *119*, 7851-7862.
- (14) Brooks, B. R.; Bruccoleri, R. E.; Olafson, B. D.; States, D. J.; Swaminathan, S.; Karplus, M. *J. Comput. Chem.* **1983**, *4*(2), 187-217.
- (15) Sakurai, M.; Murata, M.; Inoue, Y.; Hino, A.; Kobayashi, S. *Bull. Chem. Soc. Jpn.* **1997**, *70*, 847-858.
- (16) Weiner, S. J.; Kollman, P. A.; Nguyen, D. T.; Case, D. A. *J. Comput. Chem.* **1986**, *7*(2), 230-252.
- (17) Bonanno, G.; Noto, R.; Fornili, S. L. *J. Chem. Soc., Faraday Trans.* **1998**, *94*, 2755-2762.
- (18) Jorgensen, W. L.; Madura, J. D.; Swenson, C. J. *J. Am. Chem. Soc.* **1984**, *106*, 6638-6646.
- (19) Damm, W.; Frontera, A.; Tirado-Rives, J.; Jorgensen, W. L. *J. Comput. Chem.* **1997**, *18*(16), 1955-1970.
- (20) Conrad, P. B.; de Pablo, J. J. *Fluid Phase Equilib.* **1998**, *150-151*, 51-61.
- (21) Berendsen, H. J. C.; Postma, J. P. M.; Gunsteren, W. F. v.; Hermans, J. In *Intermolecular Forces*; Pullman, B., Ed.; Reidel: Dordrecht, 1981; p 331-342.
- (22) Toukan, K.; Rahman, A. *Phys. Rev. B* **1985**, *31*(5), 2645-2648.
- (23) Jorgensen, W. L.; Maxwell, D. S.; Tirado-Rives, J. *J. Am. Chem. Soc.* **1996**, *118*, 11225-11236.
- (24) Darden, T.; York, D.; Pedersen, L. *J. Chem. Phys.* **1993**, *98*(12), 10089-10092.
- (25) Essmann, U.; Perera, L.; Berkowitz, M. L.; Darden, T.; Lee, H.; Pedersen, L. G. *J. Chem. Phys.* **1995**, *103*(19), 8577-8593.
- (26) Wilding, N. B.; Binder, K. *Physica A* **1996**, *231*, 439-447.
- (27) Mehlig, B.; Heermann, D. W.; Forrest, B. M. *Phys. Rev. B* **1992**, *45*(2), 679-685.
- (28) Tuckerman, M.; Berne, B. J.; Martyna, G. J. *J. Chem. Phys.* **1992**, *97*(3), 1990-2001.
- (29) Martyna, G. J.; Tuckerman, M. E.; Tobias, D. J.; Klein, M. L. *Molecular Physics* **1996**, *87*(5), 1117-1157.
- (30) Nosé, S. *J. Chem. Phys.* **1984**, *81*(1), 511-519.
- (31) Cohen, M. H.; Grest, G. S. *Phys. Rev. B* **1979**, *20*(3), 1077-1098.
- (32) Magazú, S.; Migliardo, P.; Musolino, A. M.; Sciortino, M. T. *J. Phys. Chem.* **1997**, *101*, 2348-2351.
- (33) Banipal, P. K.; Banipal, T. S.; Lark, B. S.; Ahluwalia, J. C. *J. Chem. Soc., Faraday Trans.* **1997**, *93*(1), 81-87.
- (34) Galema, S. A.; Hoiland, H. *J. Phys. Chem.* **1991**, *95*, 5321-5326.
- (35) Magazú, S.; Maisano, G.; Middendorf, H. D.; Migliardo, P.; Musolino, A. M.; Villari, V. *J. Phys. Chem. B* **1998**, *102*, 2060-2063.
- (36) Sok, R. M.; Berendsen, H. J. C.; Gunsteren, W. F. v. *J. Chem. Phys.* **1992**, *99*(6), 4699-4704.
- (37) Gusev, A. A.; Arizzi, S.; Suter, U. W. *J. Chem. Phys.* **1993**, *99*(3), 2221-2227.
- (38) Kob, W. *J. Phys.: Condens. Matter* **1999**, *11*, R85-R115.
- (39) Gusev, A. A.; Suter, U. W. *J. Chem. Phys.* **1993**, *99*(3), 2228-2234.
- (40) Ediger, M. D.; Angell, C. A.; Nagel, S. R. *J. Phys. Chem.* **1996**, *100*, 13200-13212.
- (41) Rössler, E.; Sokolov, A. P.; Kisliuk, A.; Quitmann, D. *Phys. Rev. B* **1994**, *49*(21), 14967-14978.
- (42) Habasaki, J.; Okada, I.; Hiwatari, Y. *Phys. Rev. E* **1995**, *52*(3), 2681-2687.
- (43) Williams, M. L.; Landel, R. F.; Ferry, J. D. *J. Am. Chem. Soc.* **1955**, *77*, 3701-3706.
- (44) Soesanto, T.; Williams, M. C. *J. Phys. Chem.* **1981**, *85*, 3338-3341.